J. Fluid Mech. (1984), *vol.* 144, *pp.* 419–443
Printed in Great Britain

Surface-wave propagation over sinusoidally varying topography

By A. G. DAVIES AND A. D. HEATHERSHAW
Institute of Oceanographic Sciences, Crossway, Taunton, Somerset, TA1 2DW

(Received 14 July 1983 and in revised form 1 February 1984)

Surface waves travelling in water of finite depth may be scattered by a region of undulating bottom topography. The present study is concerned with the idealized two-dimensional situation in which long-crested surface waves are incident upon a patch of long-crested regular bottom ripples. The principal question examined concerns the amount of incident wave energy that is reflected by the ripple patch. Linear perturbation theory is used to show that the reflection coefficient is both oscillatory in the quotient of the length of the patch and the surface wavelength, and also strongly dependent upon the quotient of the surface and bed wavelengths. In particular, there is a Bragg resonance between the surface waves and the ripples, which is associated with the reflection of incident wave energy. A secondary question concerns the nature of the wave field in the immediate vicinity of the ripple patch. In resonant cases, it is shown how the partially standing wave on the upwave side of the ripple patch gives way, in an almost linear manner over the patch itself, to a progressive transmitted wave on the downwave side. The theoretical predictions are compared with an extensive set of laboratory observations made in a wave tank. Comparisons relating both to the reflection coefficient, and also to the wave field over the ripple patch, are shown to give consistently good agreement. Finally, the implications of the results for sediment transport on an erodible bed are examined.

1. Introduction

When surface waves are incident on a region of undulating seabed topography, it is well known that wave energy may be scattered by the bedforms. In general, incident waves travelling onto a bed roughness patch from any one direction may be scattered into any other direction. For large roughness patches, this problem has been treated by Long (1973), who examined the case of surface waves propagating over an arbitrary spectrum of bottom perturbations. A rather simpler situation, which is of particular interest to workers in the field of sediment transport and which is treated here, is that in which long-crested waves are incident upon purely transverse bed features. In this case, there are only two types of interaction between the waves and the bed, namely back-scatter (wave reflection) and forward-scatter (wave transmission). One reason why this problem is of interest is that, on erodible beds, there is a suggestion of a coupling between wave energy reflection and bedform growth, which may have significant implications for coastal protection.

The present study is concerned with the interaction between surface waves and a pre-existing (fixed) pattern of undulations on the bed. In practice, such a pattern may comprise shore-parallel bars (Short 1975), or tidally generated features such as sandwaves (Langhorne 1982), lying transverse to the direction of wave propagation. The study arose from some theoretical predictions (Davies 1982*a*) for the reflection

coefficient of a fixed patch of ripples on an otherwise flat bed. In the present paper, these predictions are supported by an extensive set of measurements carried out in a wave tank. (Some preliminary aspects of this investigation were described briefly by Heathershaw (1982).) In addition, in the light of some results from the experiments which were outside the scope of the original theoretical study, the theory has been extended to enable comparisons between measured and predicted wave properties both above the ripple patch (referred to as the 'near field'), and on either side of it (the 'far field').

In the two-dimensional problem considered by Davies (1982*a*), the interaction between surface waves and a patch of bottom ripples was examined on the basis of linear perturbation theory, and results were obtained for the reflected and transmitted waves for the 'far field', well away from the region of bed disturbance. Although the theory was strictly applicable only to small roughness patches, the results indicated that, in certain circumstances, very few ripples may be needed to produce a substantial back-scattered wave. Firstly, it was shown that the reflection coefficient is oscillatory in the ratio of the surface wavelength to the length of the roughness patch and, secondly, that it is resonant if the surface wavelength is twice the bed wavelength. Taken together, these two effects produce a resonant peak near this critical ratio of wavelengths, the width of which decreases, and the intensity of which increases, as the number of ripples in the patch increases. Both the oscillatory nature, and the resonance, of the reflection coefficient have been established in a number of previous related studies. The oscillatory nature has been identified by, for example, Kreisel (1949), Newman (1965), Mei & Black (1969) and Fitz-Gerald (1976) and also, for long surface waves, by Jeffreys (1944). The possible importance of the Bragg resonance was pointed out by Ursell (1947). More recently, it has been central to Long's (1973) study, it has been considered in a water-wave application by Dalrymple & Fowler (1982), and it has been discussed by various authors in a wider context (e.g. Beckmann & Spizzichino 1963; Fortuin 1970). It is believed, however, that there has been no previous attempt to combine the two effects in a single theory (see the literature review of Davies 1980).

Results for the 'near field', over the ripple patch, were presented by Davies (1982*b*). As expected from previous studies, the interaction between surface waves and sinusoidal ripples was found to give rise to two new waves with wavenumbers equal to the sum and difference of those of the surface waves and the bedforms. The theory in this paper produced a physically unrealistic result at resonance, as a result of the assumption that the ripple patch was of infinite horizontal extent; in particular, it produced an infinite reflection coefficient for bed wavelengths equal to exactly one half of the surface wavelength. The nature of this resonant interaction has been examined recently by Mitra & Greenberg (1984).

In §2 the results of the two earlier studies (Davies 1982*a*, *b*) are drawn into a single framework. Essentially, the results of Davies (1982*a*) for the 'far field' are extended to some considerations of the 'near field', but for a physically realistic ripple patch of finite extent. In §2.1 the formulation is discussed, and the problem of progressive waves incident upon a patch of sinusoidal ripples is considered. Throughout the study, two particular cases are treated. In the first case, the incident waves are assumed to undergo no attenuation in amplitude as they travel across the ripple patch. This amounts to the use of the theory in a pure form; but, in cases in which there is a substantial reflected wave, it results in an imbalance between the incident, reflected and transmitted wave-energy fluxes. The second case treated is that in which an energy balance is imposed on the solution by an approach suggested by Davies (1982*a*). This assumes, with good justification as it turns out, that the attenuation

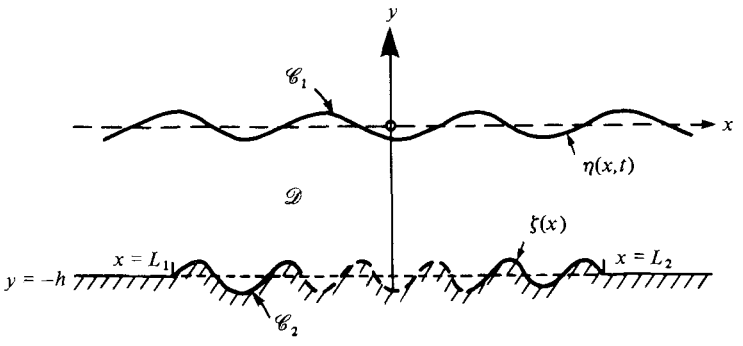

FIGURE 1. Definition sketch.

of the incident-wave amplitude is a linear function of distance across the ripple patch. In §2.2 the wave reflection coefficient is discussed and results for the surface elevation are presented. Since we are concerned with an irrotational theory, we take no account of the presence of the (thin) wave boundary layer above the impermeable bed. More importantly, we assume that the flow above the ripples is always non-separating (see §5.1). In §3 the experimental set-up is described, and in §4 the results are presented. Initially in §4, results for the reflection coefficient are compared with theoretical predictions. Next, measured elevations throughout the wave tank are examined. Finally, in §5, the results are discussed, and their implications for bedform stability and sediment movement are considered.

2. Theory

2.1. *Formulation*

As depicted in figure 1, the bed surface is assumed to comprise a patch of periodic, two-dimensional, ripples on an otherwise flat bed, in water of constant mean depth h. It is assumed that the flow is two-dimensional and irrotational, so that Laplace's equation is satisfied in $\mathscr{D}$ by the velocity potential $\phi(x, y, t)$:

$$\nabla^2\phi = 0 \quad \text{in} \quad \mathscr{D}. \tag{1}$$

The departure of the water surface from its mean level ($y = 0$) is taken as $\eta(x, t)$, and that of the bed surface from its mean level ($y = -h$) as $\zeta(x)$. The steady-state results obtained here are based upon perturbation expansions of ϕ, η and ζ, in powers of a small parameter ϵ, which is later identified with ratios of the various lengthscales in the problem:

$$\phi = \epsilon\phi_1 + \epsilon^2\phi_2 + \ldots, \quad \eta = \epsilon\eta_1 + \epsilon^2\eta_2 + \ldots, \quad \zeta = \epsilon\zeta_1 + \epsilon^2\zeta_2 + \ldots. \tag{2}$$

In this approach, bottom-topography variations are regarded as small perturbations on a plane surface. In particular, from the condition that the component of fluid velocity normal to the bed must vanish on the boundary, the interaction between the (first-order) flow, which would be present without the boundary perturbations, and the perturbations themselves, is treated as a new source of (second-order) fluid motion situated on the plane surface.

The exact boundary conditions at the free surface and the bed are as follows:

$$\eta_t + \phi_y - \phi_x\eta_x = 0 \quad \text{on} \quad \mathscr{C}_1, \tag{3}$$

$$g\eta - \phi_t + \tfrac{1}{2}(\phi_x^2 + \phi_y^2) = 0 \quad \text{on} \quad \mathscr{C}_1, \tag{4}$$

$$\phi_y - \phi_x\zeta_x = 0 \quad \text{on} \quad \mathscr{C}_2, \tag{5}$$

where t is the time, g is the acceleration due to gravity, and the subscripts indicate differentiation. In the approach adopted here, the kinematical conditions (3) and (5), and the pressure condition (4), are satisfied at the mean surface and bed levels $y = 0$ and $y = -h$ respectively, by the introduction of Taylor expansions. In particular, (2) are used to reduce the original nonlinear problem to a series of linear problems, the first to order ϵ, the second to order ϵ^2, and so on (see Davies 1980).

The governing equation and boundary conditions, correct to order ϵ, are

$$\nabla^2\phi_1 = 0 \quad \text{in} \quad -h \leqslant y \leqslant 0, -\infty < x < \infty, \tag{6}$$

$$\eta_{1t} + \phi_{1y} = 0 \quad \text{on} \quad y = 0, \tag{7}$$

$$g\eta_1 - \phi_{1t} = 0 \quad \text{on} \quad y = 0, \tag{8}$$

$$\phi_{1y} = 0 \quad \text{on} \quad y = -h. \tag{9}$$

The problem, correct to order ϵ^2, is made up of two separable parts. One is well known (see e.g. Peregrine 1972) as Stokes' theory to the second order of approximation, and it concerns the steepening of the surface wave crests and the flattening of the troughs, above a bed which is flat. The other expresses the interaction between the first-order motion $O(\epsilon)$ and the undulations $O(\epsilon)$ on the bed. It is the solution of this second part of the problem that is relevant here. The governing equation and boundary conditions, correct to order ϵ^2, are therefore taken as follows:

$$\nabla^2\phi_2 = 0 \quad \text{in} \quad -h \leqslant y \leqslant 0, -\infty < x < \infty, \tag{10}$$

$$\eta_{2t} + \phi_{2y} = 0 \quad \text{on} \quad y = 0, \tag{11}$$

$$g\eta_2 - \phi_{2t} = 0 \quad \text{on} \quad y = 0, \tag{12}$$

$$\phi_{2y} + \zeta_1\phi_{1yy} - \phi_{1x}\zeta_{1x} = 0 \quad \text{on} \quad y = -h. \tag{13}$$

The boundary conditions at the free surface, (11) and (12), are as in the problem $O(\epsilon)$, while in (13) the effect of the rippled bed is apparent. The governing equation and boundary conditions $O(\epsilon^3)$, which are not stated here, have been discussed by Davies (1980).

The bed surface depicted in figure 1 is prescribed, to order ϵ, about its mean level ($y = -h$) as

$$\zeta_1(x) = \begin{cases} 0 & \text{in} \quad -\infty < x \leqslant L_1, \\ Y(x) & \text{in} \quad L_1 \leqslant x \leqslant L_2, \\ 0 & \text{in} \quad L_2 \leqslant x < \infty. \end{cases} \tag{14}$$

It follows that (13) may be rewritten as follows:

$$\phi_{2y} = \begin{cases} 0 & \text{in} \quad -\infty < x < L_1, \\ -V_0(x,t) & \text{in} \quad L_1 < x < L_2, \\ 0 & \text{in} \quad L_2 < x < \infty \end{cases} \quad \text{on} \quad y = -h, \tag{15}$$

where

$$V_0(x,t) = -\phi_{1x}(x, -h, t)\, Y_x + \phi_{1yy}(x, -h, t)\, Y. \tag{16}$$

The effects on the fluid as a whole of this vertical velocity perturbation at the bed are described by (10)–(12). By the nature of the problem, it is required that the waves in the perturbation solution satisfy the radiation condition; in other words, these waves are required to be outgoing from the region of bed disturbance.

If we prescribe ϕ_1 as a periodic function of time and seek a steady-state solution of (10)–(13), we find, for reasons that are well known, that this solution is indeterminate. We therefore employ the device (Lamb 1932, Art. 232) of introducing into the formulation a small amount of friction proportional to the relative velocity. Although the coefficient of friction μ is set ultimately to zero, the device ensures the convergence of the integrals arising in the analysis, and it clarifies the way in which the radiation condition can be satisfied.

We assume further that ϕ_2 is bounded and also that ϕ_2, and its first and second derivatives, tend to zero as $|x| \to \infty$ in such a way that Fourier transforms exist in x; the inclusion in the analysis of the linear friction term justifies the latter assumption. If Fourier transforms are taken of the governing equation (10) and of the boundary conditions, and if the solution is made specific to waves of frequency σ, it may be shown that the inverse transform of the velocity potential is such that $\phi_2(x, y, t)$ is given by

$$\phi_2(x, y, t) = \int_{-\infty}^{\infty} \frac{g\xi \cosh(\xi y) + (\sigma^2 - \mathrm{i}\mu\sigma) \sinh(\xi y)}{2\pi\xi\{(\sigma^2 - \mathrm{i}\mu\sigma) \cosh(\xi h) - g\xi \sinh(\xi h)\}} A(\xi)\, \mathrm{e}^{\mathrm{i}\{\sigma t - \xi x\}}\, \mathrm{d}\xi, \tag{17}$$

where ξ is the transform variable and

$$A(\xi)\, \mathrm{e}^{\mathrm{i}\sigma t} = -\int_{L_1}^{L_2} V_0(x, t)\, \mathrm{e}^{\mathrm{i}\xi x}\, \mathrm{d}x. \tag{18}$$

The general integral (17) determines the solution for both the 'near' and 'far' fields. If, for convenience, $V_0(x, t)$ is taken as the real part of a complex function, this results in a complex form for ϕ_2, from which the required velocity potential is obtained by taking the real part.

The particular form of the function $A(\xi)$ depends upon both the nature of the bedforms and the unperturbed first order motion. First, we assume the bedforms to be sinusoidal ripples such that $Y(x)$ in (14) is given by

$$Y(x) = b \sin(lx + \delta), \tag{19}$$

where b is the ripple amplitude, l is the ripple wavenumber and δ is an arbitrary phase angle. For continuity of bed elevation at the ends of the roughness patch, we write

$$L_2 = L = \frac{m\pi}{l}, \quad L_1 = -L = -\frac{m\pi}{l}, \quad \delta = 0, \tag{20}$$

where m is an integer. Thus there are m ripples in the patch, which is centred on $x = 0$ and is of length $2L$. Secondly, we assume, at least initially, that the incident waves in the solution, to order ϵ, are given by

$$\eta_1 = a \sin(kx - \sigma t), \tag{21}$$

where a, k and σ are the surface-wave amplitude, wavenumber and frequency, respectively. The corresponding velocity potential satisfying (6)–(9) is given by

$$\phi_1 = \frac{ga}{\sigma} \frac{\cosh\{k(y + h)\}}{\cosh(kh)} \cos(kx - \sigma t), \tag{22}$$

where σ is related to h and k by the dispersion relation

$$\sigma^2 = gk \tanh(kh). \tag{23}$$

(It is important to note that the dispersion relation (23) is still valid in the solution to order ϵ^2.)

The function $A(\xi)$ may be obtained on the basis of (18) from (14), (16), (19), (20) and (22). The perturbation potential ϕ_2 may then be obtained for both the near and far fields, subject to the condition that solutions for the far field must only comprise waves satisfying the radiation condition as $x \to \pm\infty$. If the amplitudes of these outgoing waves are not small compared with the amplitude a of the incident wave in the first-order solution, then the velocity potential correct to second order $(\phi_1+\phi_2)$ will, in general, violate the overall requirements of energy conservation in the solution. Strictly, in the assumed absence of any mechanisms of dissipation, the incident wave-energy flux must be balanced by the reflected and transmitted energy fluxes. A procedure to impose an energy balance on the solution was proposed by Davies (1982*a*), in which the surface-wave amplitude in the first-order solution was assumed to decrease linearly from its starting value a at $x = -L$ to a new lower value at $x = +L$. There is strong justification for this assumption of linear attenuation of wave amplitude across the ripple patch, at least in resonant cases, both from the results for the wave-reflection coefficient (see §2.2.1) which indicate a linear increase in the reflected wave amplitude a_R with the number of ripples in the patch, and also from the later experimental results (see §4). Details of the implementation of the procedure to impose an energy balance have been discussed by Davies (1982*a*) and Davies & Heathershaw (1983).

The integral in (17) has been evaluated by contour-integration procedures. Initially, the transform variable ξ has been taken as the real part of a complex variable $\lambda = \xi + i\chi$, and the path of integration $-\infty < \xi < \infty$ has been replaced by a closed contour in the λ-plane. This contour has been chosen as a semicircle of radius r, which includes the portion $-r < \xi < r$ of the real axis of λ, and is taken in either the upper or lower half-plane such that a physically admissible solution is obtained. Ultimately, as $r \to \infty$, the required path of integration, namely the ξ-axis, becomes part of the complete contour. Since the semicircular portion of the contour makes a contribution to the solution which tends to zero as $r \to \infty$ (see Davies 1980), the required result for the velocity potential is simply equal to the result obtained by integrating around the complete contour. In practice, it is necessary to separate the integral in (17) into two parts I_1 and I_2 and to make an appropriate choice of contour for each part, such that a physically admissible solution is obtained in each of the regions $x < -L$, $|x| < L$ and $x > L$. (The integrand of $I_1 \sim \exp\{-\chi(L-x)\}$ and of $I_2 \sim \exp\{\chi(L+x)\}$.) The role of the linear friction term at this stage in the argument is to displace certain singularities of each integrand either into, or out of, the chosen contours. This occurs in such a way that, ultimately, bounded solutions satisfying the radiation condition are obtained as $\mu \to 0$.

In summary, for the general case in which $l \neq 2k$ (and as $\mu \to 0$), the perturbation solution comprises the various parts shown in diagrammatic form in figure 2. Here each arrow represents a propagating wave mode, and against each arrow is indicated the pole position in the λ-plane with which the wave is associated. The pole position governs the wavenumber of each mode, and also the direction of travel of the wave (as indicated by the arrow head). Note that, from integral I_1, there is a wave associated with the pole at $-k$ which travels off the patch in the negative x-direction. Similarly, from integral I_2, there is a wave associated with the pole at $+k$ which travels off the patch in the positive x-direction. In $|x| < L$ there are contributions from these two poles, as well as from the poles at $k \pm l$. The sum $(k+l)$-wave travels always in the onward transmitted direction, while the difference $(k-l)$-wave travels either in the onward transmitted direction or is back-reflected, depending upon whether its wavelength is respectively less than or greater than that of the ripples.

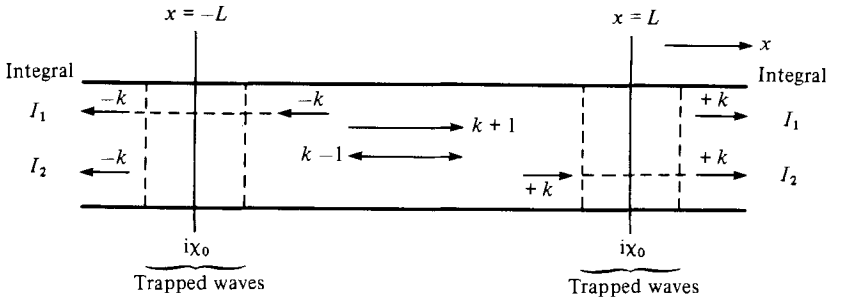

FIGURE 2. Wave modes in the perturbation solution for the general case in which $l \neq 2k$. Each arrow represents a propagating wave mode, and against each arrow is indicated the pole position with which it is associated. The direction of travel is indicated by the arrow head. The trapped wave modes are confined to the regions near the ends of the ripple patch.

The poles on the imaginary axis of λ (labelled $i\chi_0$), which are associated with trapped waves centred on both ends of the ripple patch, ensure the smooth continuation of the solution at $x = \pm L$. It remains only to determine the residues of the poles identified above; the procedures involved have been discussed in detail by Davies & Heathershaw (1983).

As $l \to 2k$ the position of the pole at $\lambda = k - l$ tends towards that of the pole at $\lambda = -k$. In this special case it is necessary to recalculate the results both for the region upwave of the ripple patch ($x < -L$), and for the region of the ripple patch itself ($|x| < L$). On the downwave side of the ripple patch ($x > L$), the solution is independent of the poles at $\lambda = -k$ and $\lambda = k - l$, and the result for the general case in which $l \neq 2k$ remains unaltered.

2.2. *Theoretical results*

2.2.1. *The reflection coefficient*

We state initially results which are obtained from the asymptotic behaviour of the solution for the potential ϕ_2 as $x \to -\infty$ and as $x \to +\infty$. In particular, we define the wave-reflection coefficient from the potential of the outgoing perturbation waves in $x < -L$ and from the incident waves in the first-order solution. For the general case in which $l \neq 2k$ and in which the incident waves are unattenuated over the ripple patch, the former waves are given in the limit $x \to -\infty$ by the real part of

$$\phi_2(x, y, t) = \frac{2\cosh\{k(y+h)\}}{2kh + \sinh(2kh)} \frac{C_*(-1)^m 2k/l}{(2k/l)^2 - 1} \sin(2kL)\, e^{i(\sigma t + kx)}, \tag{24}$$

where

$$C_* = \frac{gabk}{\sigma \cosh(kh)}.$$

The reflection coefficient K_R is then defined as the quotient of the coefficient of $\cos(\sigma t + kx)$ in (24) and the equivalent coefficient for the incident waves in (22), such that

$$K_R = \frac{a_R}{a} = \frac{2bk}{2kh + \sinh(2kh)} \frac{(-1)^m 2k/l}{(2k/l)^2 - 1} \sin(2kL) \quad (l \neq 2k). \tag{25}$$

For the special case in which $l = 2k$, the reflection coefficient becomes

$$K_R = \frac{2bk}{2kh + \sinh(2kh)} \frac{m\pi}{2} \quad (l = 2k). \tag{26}$$

Equivalent results may be obtained for incident waves that are attenuated over the ripple patch. These results differ significantly from those given by (25) and (26) only if $K_R \gtrsim 0.4$.

From (26) it may be noted that, at resonance when $l = 2k$, the reflection coefficient increases linearly in the number of ripples (m) in the patch. For this reason, the earlier assumption of linear attenuation of incident-wave amplitude across the patch is reasonable, at least near to resonance. More generally, (25) reveals that, while the maximum value of K_R is found near the critical ratio of wavenumbers $2k/l = 1$, the reflection coefficient is also oscillatory in the ratio of the length $2L$ of the ripple patch to the surface wavelength.

As far as the outgoing waves on the downwave side of the ripple patch are concerned, it may be shown that, for incident waves that are unattenuated over the patch, the potential in the asymptotic limit $x \to +\infty$ is given by

$$\phi_2(x, y, t) = 0. \tag{27}$$

It follows from (24) and (27) that the perturbing vertical velocity distribution prescribed at the bottom boundary is such as to produce an outgoing wave in the upwave direction only. However, in the case of attenuated incident waves, there is a small outgoing wave on the downwave side, the properties of which have been discussed by Davies (1982*a*).

2.2.2. *Properties of the waves over the ripple patch*

In considering the properties of the waves over the ripple patch, we utilize the complete solution in $-\infty < x < \infty$. The elevation of the first-order incident waves is given by (21), and the elevation $\eta_2(x, t)$ in the perturbation solution is obtained from (12) (only the real part of which is of interest). In figures 3 and 4 we show results for a typical case near to resonance which relates to one of the later laboratory experiments. The parameter settings are as follows: ripple amplitude $b = 5$ cm, ripple wavelength $\lambda_R = 2\pi/l = 100$ cm, the number of ripples $m = 10$, the water depth $h = 41.7$ cm, and the wave period $T = 2\pi/\sigma = 1.23$ s, from which it follows from (23) that $2k/l = 0.985$. The incident waves are assumed to be unattenuated across the ripple patch, and so, from (25), the reflection coefficient is $K_R = 0.509$.

In both figures 3 and 4, results for the normalized elevation $\eta(x, t)/a$ have been expressed in the form

$$\frac{\eta(x, t)}{a} = E_1(x) \cos(\sigma t) + E_2(x) \sin(\sigma t). \tag{28}$$

The curves plotted in figure 3 are for the perturbation solution only, and show the instantaneous elevations $E_1(x)$, $E_2(x)$, $-E_1(x)$ and $-E_2(x)$, at the phase angles $\sigma t = 0$, $\frac{1}{2}\pi$, π and $\frac{3}{2}\pi$ respectively, together with the envelope curves for wave elevation given by $\pm(E_1^2 + E_2^2)^{\frac{1}{2}}$. The results show that, on the downwave side of the ripple patch ($x > L$), the water surface is motionless as required by (27). Between the downwave end of the patch ($x = L$) and the upwave end ($x = -L$), the perturbation wave increases in size. Thereafter, in $x < -L$, the wave propagates away from the ripple patch in the negative x-direction. The result of superimposing the perturbation waves and the incident waves is shown in figure 4. The evolution of a partially standing-wave pattern is apparent in $|x| < L$, with a fully developed partially standing wave being present in $x < -L$. At the ends of the patch ($x = \pm L$), a smooth transition in the solution is obtained as a result of the trapped wave modes associated with the poles on the imaginary axis of λ (see figure 2). The detailed properties of these trapped

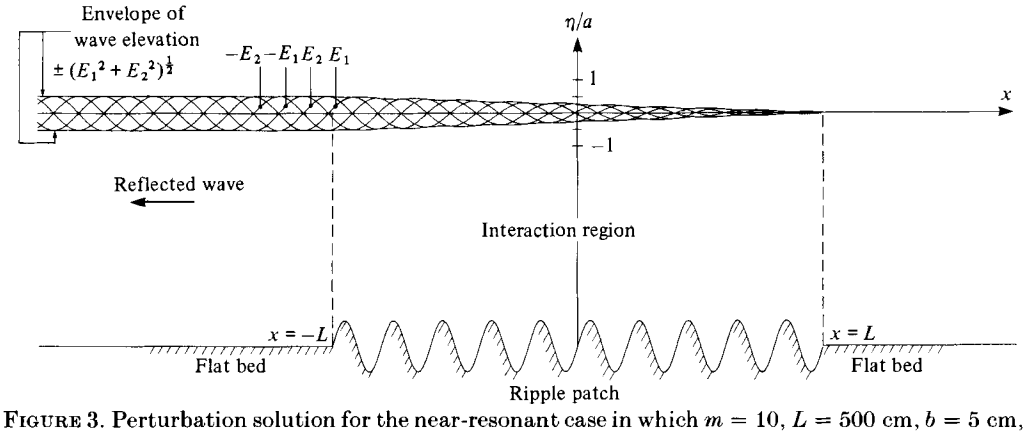

FIGURE 3. Perturbation solution for the near-resonant case in which $m = 10$, $L = 500$ cm, $b = 5$ cm, $\lambda_R = 100$ cm, $h = 41.7$ cm and $T = 1.23$ s ($2k/l = 0.985$). The development of the reflected wave in the interaction region is illustrated by the instantaneous surface wave profiles $\pm E_1$, $\pm E_2$ (see (28)), and by the envelope of wave elevation $\pm (E_1^2 + E_2^2)^{\frac{1}{2}}$. There is an almost linear increase in the reflected wave amplitude between $x = +L$ and $x = -L$. Thereafter, in $x < -L$, the reflected wave is an outgoing wave, with amplitude $a_R = 0.509a$.

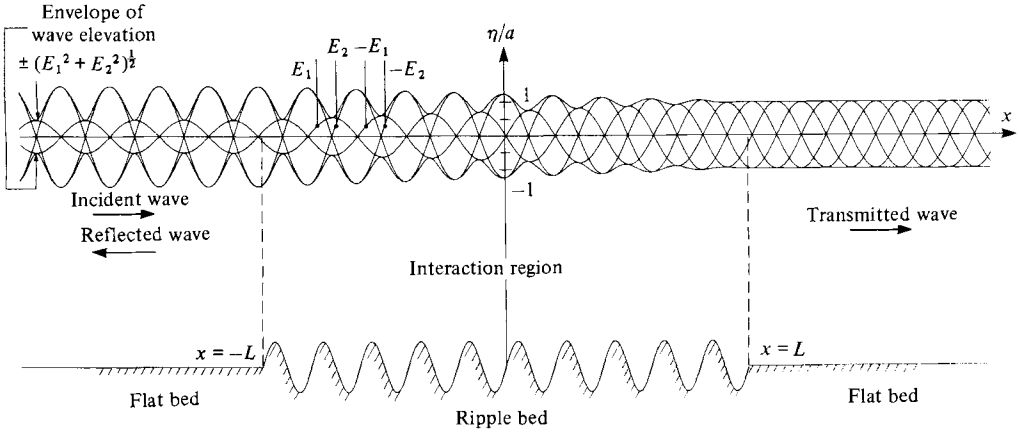

FIGURE 4. Superimposition of the first order and perturbation solutions (see figure 3 for the perturbation solution) for the near-resonant case in which $m = 10$, $L = 500$ cm, $b = 5$ cm, $\lambda_R = 100$ cm, $h = 41.7$ cm and $T = 1.23$ s ($2k/l = 0.985$). The instantaneous profiles of wave elevation $\pm E_1$, $\pm E_2$ (see (28)) are plotted, together with the envelope of wave elevation $\pm (E_1^2 + E_2^2)^{\frac{1}{2}}$. The development of a partially standing-wave structure between $x = +L$ and $x = -L$ is evident.

modes have been illustrated by Davies & Heathershaw (1983). In the example in figures 3 and 4, their combined effect at both ends of the patch ($x = \pm L$) is of the order of 1 % of the amplitude of the incident wave.

2.4.3. *Limitations on the solution*

There are certain physical limitations on the solution which arise both on account of terms dropped in linearizing the boundary conditions, and also on account of the general requirement of the method that $|\phi_2| \ll |\phi_1|$. The limitations of the former kind have been discussed in detail by Davies (1980, 1982*b*) and may be stated as a set of simple conditions on the various lengthscales in the problem, namely

$$ak, \quad \frac{a}{h}, \quad \frac{a}{k^2h^3}, \quad bl, \quad \frac{b}{h}, \quad bk \ll 1. \tag{29}$$

The small parameter ϵ introduced in (2) to set up a basic hierarchy of terms in the solution is connected with the smallness of each of the parameters listed. However it is not necessary, or possible, to identify ϵ with any one of these parameters, and it is not a requirement of the method of solution that this be done. In addition to the above conditions, the analysis breaks down if $k \gg l$.

The latter limitation, $|\phi_2| \ll |\phi_1|$, imposes at the outset a condition on the size of the reflected wave. In its pure form, the theory requires both the reflected and transmitted waves in the perturbation solution to be small compared with the incident wave. However, if an energy balance is imposed on the solution, this condition may be relaxed to some extent (see §2.1). In general, the first estimate of a_R from the pure theory should be viewed as providing an upper bound on the size of the reflected wave; in practice, it is necessary to correct first estimates of a_R only in resonant cases for which the reflection coefficient is large ($K_R \gtrsim 0.4$). It should be noted here that the perturbation solution may predict over-reflection; particular care should be exercised in interpreting any results that suggest that $|a_R| > a$. Finally, the present theory is limited by ignoring the effects of energy dissipation by bottom percolation and bottom friction. Despite these limitations however, the theory is applicable in a variety of physically interesting cases, including the laboratory experiments described in §§3 and 4.

3. Experimental techniques

3.1. *Construction of the ripple patch*

To test the results of §2, and in particular (25) and (26), measurements were carried out by one of the authors (ADH) during a visit to the US Army Corps of Engineers, Coastal Engineering Research Center, Fort Belvoir, Virginia, USA. The tests were carried out in a glass-walled wave tank, 45.72 m × 0.91 m × 0.91 m (nominally 150 ft × 3 ft × 3 ft). A wavelength of 1 m was chosen for the ripples, and a patch of ripples was built into a false bottom in the tank (figure 5). This wavelength gave resonant-wave periods approximately in the centre of the range which could reasonably be tested (about 0.5–3.0 s), and thus permitted a detailed examination of the oscillatory nature of the reflection coefficient. The amplitude of the ripples was chosen to be 5 cm (a trough-to-crest height of 10 cm). Initially, 10 ripples were built in the tank, with later tests being carried out on 4, 2 and 1 ripples. As ripples were removed from the patch (see figure 5), they were replaced by plywood-covered, and sand-filled, sections of false bottom. There was no facility for return flow through the false bottom.

At the end of the tank, a 1:10 slope rubberized-fibre wave-absorbing beach was built to prevent waves from being back-reflected onto the ripple patch. The beach was constructed so that, at the highest water level examined, the longest-period waves would have to travel over about twice their own wavelength of beach material. Shorter-period waves were expected to be more readily absorbed by the beach than these long-period waves.

3.2. *The wave generator*

Monochromatic sinusoidal waves were generated using an electrohydraulic piston-type wave generator. Wave period settings could be adjusted in increments of 0.01 s, and independent checks on the accuracy of these settings were carried out in the range 0.6–3.0 s by timing 30 oscillations of the wave generator bulkhead. The results of this investigation indicated agreement to within ± 0.005 s of the nominal wave-period

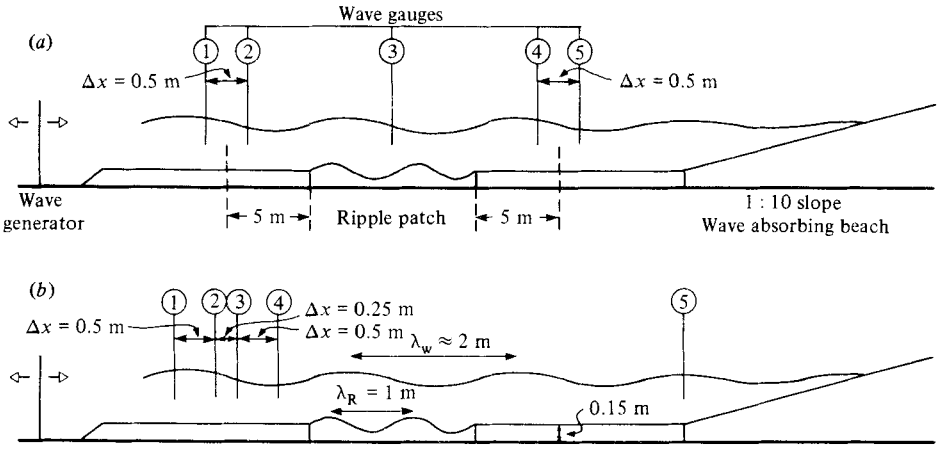

FIGURE 5. Schematic diagram showing the positions of the wave gauges in relation to the ripple patch and the beach for (*a*) measurements of the reflection coefficients of the ripple patch and the beach, and (*b*) measurements of the wave field throughout the wave tank.

setting. Following a change in the setting, the time taken for the wave system in the tank to attain a steady state was usually of the order of 60 s. Since the time between successive sets of measurements was in general longer than this (of the order of 3 min), the measurements described in §4 were representative of equilibrium conditions.

3.3. *Wave measurements*

Measurements of incident-, reflected- and transmitted-wave elevations were made using CERC-type wave gauges, which were of the parallel-wire resistance type and had a linear output (Kellum 1956; Stafford 1972). Two sizes of gauge were used. Measurements on 10 ripples, and with water depths in the range 25.0–62.5 cm, were made with gold-plated brass-wire gauges having a nominal length of 50.0 cm and a wire spacing of approximately 3.7 cm. The wire diameter was approximately 0.25 cm. For measurements on 4, 2 and 1 ripples and with water depths in the range 12.5–50.0 cm, miniature stainless-steel wire gauges were used. These had nominal wire lengths of 13.0 cm, with a wire separation of 1.5 cm and wire diameters of approximately 0.10 cm. Comparisons between the small and large gauges showed good agreement.

To determine reflection coefficients, the method described by Goda & Suzuki (1977), which involves the synchronous measurement of surface elevations with a gauge pair, was employed. Incident and reflected wavetrains are ideally resolved by a pair of wave gauges having a spacing Δx of $0.25\lambda_w$, where λ_w is the surface wavelength. In this work, gauge spacings were maintained in the range $0.15 < \Delta x/\lambda_w < 0.35$. Two pairs of gauges and a single gauge were used to make two types of measurement:

(*a*) measurements of the reflection coefficient both at a fixed point on the upwave side of the ripple patch, approximately midway between it and the wave generator, and also at a fixed point on the downwave side of the patch, approximately midway between it and the beach, with the fifth (single) gauge positioned midway along the patch;

(*b*) measurements of the variation in the reflection coefficient, and in the wave height, over the entire ripple patch and on either side of it, with the fifth gauge positioned at the foot of the beach.

These two arrangements are illustrated schematically in figure 5. In each case,

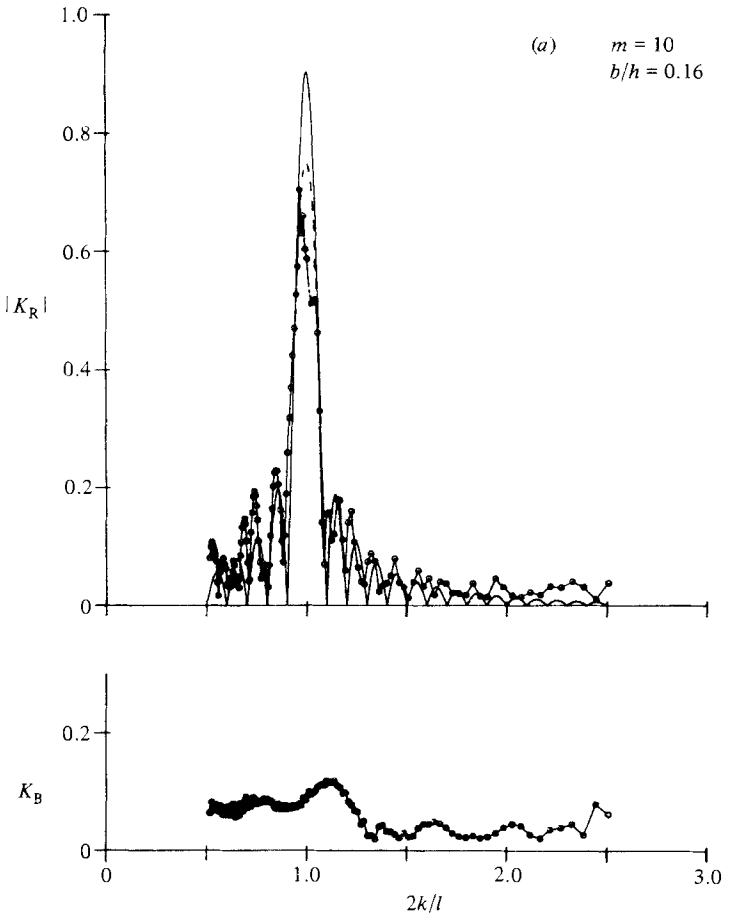

FIGURE 6(a). For caption see p. 432.

synchronous wave records were obtained by sampling each gauge 16 times per second (16 Hz) for 64 s, thus yielding 1024 data points for subsequent analysis by the fast-Fourier-transform (FFT) method. Spectral coefficients were then combined to yield a reflection coefficient for each gauge pair.

4. Experimental results

4.1. *The reflection coefficient of the patch of ripples*

Initially, we consider results for the magnitude of the reflection coefficient K_R, for which wave measurements were made with a gauge pair positioned approximately midway between the wave generator and the upwave end of the ripple patch. The variation of $|K_R|$ with the ratio of the surface and ripple wavenumbers is shown in figure 6 for $m = 10$, 4 and 2 ripples. Where practicable, the quotient $2k/l$ was varied through the range (0.5, 2.5) in steps of 0.01 for $m = 10$ and 4, and in steps of 0.02 for $m = 2$. The appropriate theoretical predictions for K_R are given by (25) and (26).

In figure 6(*a*) the measured values of $|K_R|$ for $m = 10$ ripples follow quite closely the general trend of the theoretical predictions. The width of the main resonant peak is confirmed, and agreement is reasonable for values of $2k/l$ up to about 2. For the cases of $m = 4$ and 2 ripples (figures 6*b*, *c*) the theoretical predictions are again well

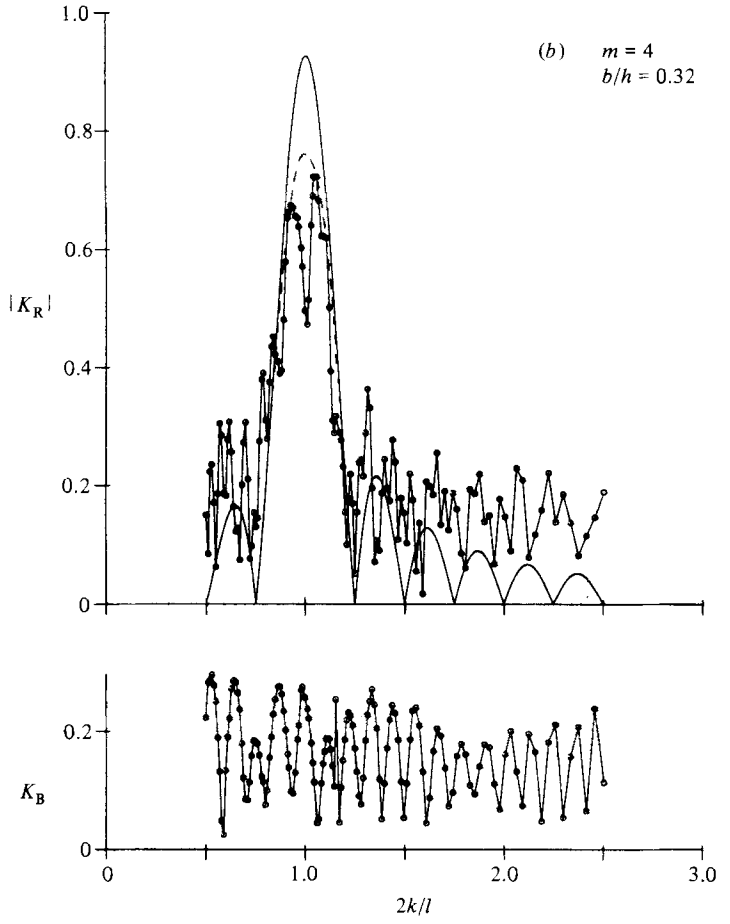

FIGURE 6(*b*). For caption see p. 432.

supported by the measurements, particularly in respect of the main resonant peaks. However, there is generally more scatter in these cases, probably due to wave-energy reflection by the beach. This question is discussed below. In each of figures 6(*a–c*), the experimental results are compared with theoretical predictions for incident waves which are assumed to be unattenuated and linearly attenuated (see §2.1), over the ripple patch. In what follows, we refer to such results as being based upon *uncorrected* and *corrected* theory respectively. In the region of the main resonant peaks in figures 6(*a–c*), better agreement is achieved between the measurements and the corrected, rather than the uncorrected, theory, as expected.

Figures 6(*a–c*) also show the reflection coefficients for the beach, for which wave measurements were made with a gauge pair positioned approximately midway between the beach and the downwave end of the ripple patch. For the case of $m = 10$ ripples, reflection coefficients for the beach were of the order of $K_B \approx 0.1$, or less, corresponding to about 1 % in terms of incident wave energy. Tests on 4 and 2 ripples showed that measured reflection coefficients were in general of the order of $K_B \approx 0.2$, or about 4 % in terms of energy. In the present context, the importance of wave reflection by the beach is that it introduces uncertainty into values of the reflection coefficient $|K_R|$ based upon measurements made on the upwave side of the ripple patch. It has been shown by Davies & Heathershaw (1983) that the magnitude of

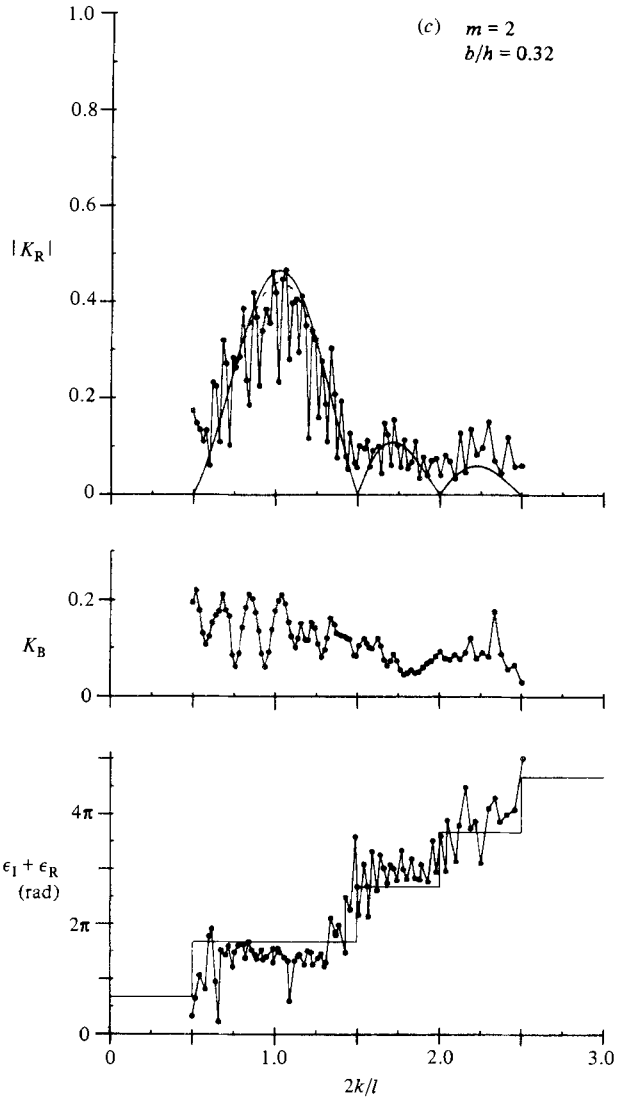

FIGURE 6. Results for the reflection coefficients both of the ripple patch ($|K_R|$) and of the beach (K_B) for: (*a*) $m = 10$ ripples ($b/h = 0.16$); (*b*) $m = 4$ ripples ($b/h = 0.32$); (*c*) $m = 2$ ripples ($b/h = 0.32$). The solid and broken curves represent the predictions of the uncorrected and corrected theory respectively. Estimates of the sum of the phase angles $\epsilon_I + \epsilon_R$ are shown for the case of $m = 2$ ripples.

the true reflection coefficient of the ripple patch, K_{RT} say, has been estimated in the experiments only to within a range of uncertainty around the measured value, K_{RM} say, given by $K_{RT} = K_{RM} \pm K_{BM}$, where K_{BM} is the measured reflection coefficient of the beach (and in which the lower bound is replaced by $K_{RT} = 0$ if $K_{BM} > K_{RM}$). This result is consistent with the differences between experiment and theory in figure 6. Re-reflection of waves by the wave generator is irrelevant in this connection, provided that equilibrium conditions have been attained in the wave tank (see §3.2). Such re-reflected waves merely contribute to the incident wave.

Figure 6 (*c*) shows the results of wave phase angle calculations made for the system

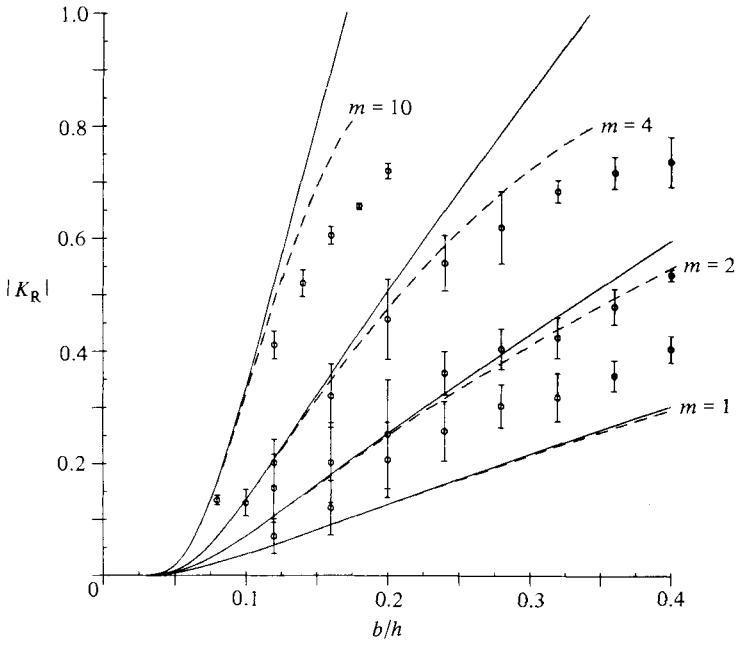

FIGURE 7. Variation of the measured mean value of $|K_R|$, at or near resonance ($2k/l \approx 1$), as a function of the quotient b/h of the ripple amplitude b and the water depth h, and for different numbers of ripples m. Error bars denote plus or minus one standard deviation from the mean.

of incident and reflected waves measured up-wave of the ripple patch in the case of $m = 2$ ripples. For incident (I) and reflected (R) waves travelling in the $+x$- and $-x$-directions, in water of constant depth h, the respective surface elevations may be expessed by

$$\eta_I = a_I \cos(kx - \sigma t + \epsilon_I), \quad \eta_R = a_R \cos(kx + \sigma t + \epsilon_R),$$

where the amplitude and phase angle of the incident wave are a_I and ϵ_I, and of the reflected wave are a_R and ϵ_R, and where h, k and σ are related by (23). It is simply demonstrated that π-phase shifts in the sum of the phase angles $\epsilon_I + \epsilon_R$ are associated with sign changes in the reflection coefficient K_R as defined by (25). For the case in which $m = 2$, the theory suggests that the sum $\epsilon_I + \epsilon_R$ should remain constant in $0.5 < 2k/l < 1.5$, that there should be π-phase shifts at either end of this range, constant values of the sum in $0 < 2k/l < 0.5$ and $1.5 < 2k/l < 2.0$ and, thereafter, for increasing $2k/l$, further π-phase shifts at $2k/l = 2.0, 2.5, 3.0, \ldots$. It may be observed in figure 6(*c*) that $\epsilon_I + \epsilon_R$ remains reasonably constant in the range $0.67 < 2k/l < 1.31$, and also in the range $1.6 \lesssim 2k/l < 1.93$, and that phase shifts occur in the ranges $0.5 \lesssim 2k/l \lesssim 0.6$ and $1.45 \lesssim 2k/l \lesssim 1.55$. Although these phase shifts are not at discrete values of $2k/l$, probably due to the presence of the reflected wave from the beach, there is a strong suggestion of the predicted behaviour of $\epsilon_I + \epsilon_R$, as indicated by the solid-line step function.

Next, we consider results for resonant cases in which $2k/l \approx 1$. In the experimental trials, time did not permit detailed measurements of $|K_R|$ over an extensive range of values of $2k/l$ for each combination of values of b/h and m examined. So, in order to determine peak values of $|K_R|$ for given b/h and m, measurements were made over only a limited range of values in the vicinity of the main resonant peak, centred on

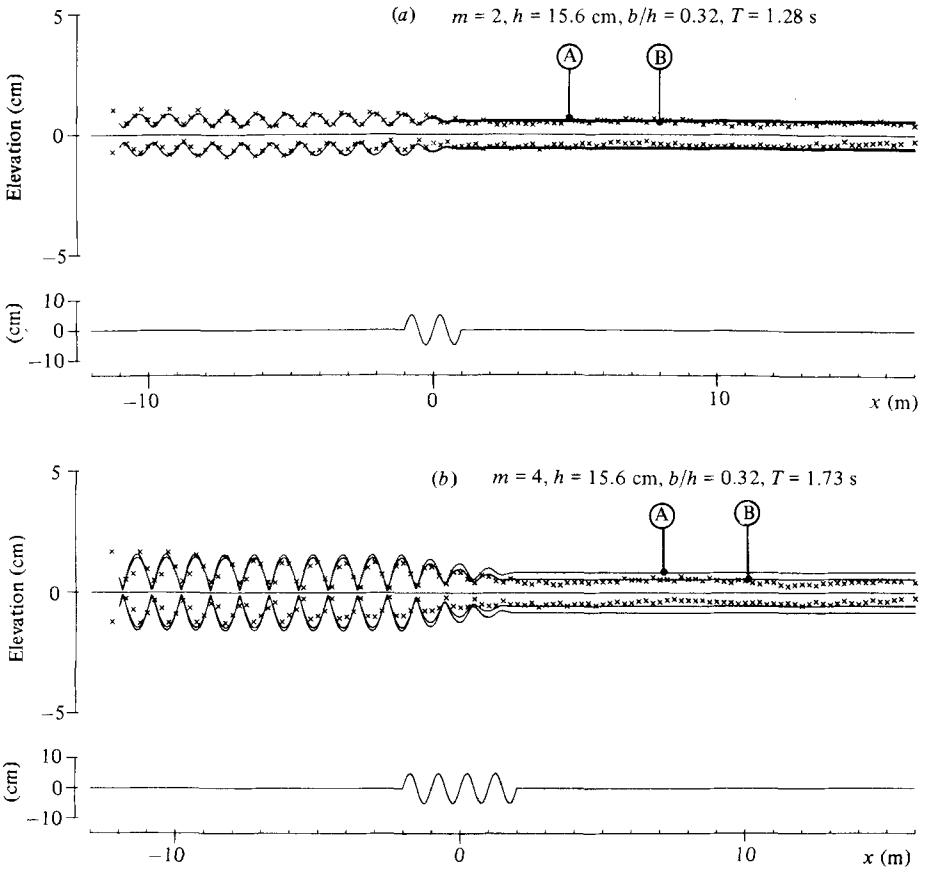

FIGURE 8(*a*, *b*). For caption see facing page.

$2k/l = 1$ and representing, in each case, $\pm 10\,\%$ of the total width of the peak. The results shown in figure 7 are means and standard deviations of the measured $|K_R|$-values lying within these ranges, and they are compared with both uncorrected, and corrected, theoretical predictions for the maximum reflection coefficient. For $m = 10$ ripples the averaged peak values underestimate the predictions of the corrected theory somewhat, for example by about 15 % for $b/h = 0.18$. For $m = 4$ and 2 ripples the averaged values give generally good agreement with the corrected theory. However, for $m = 1$ ripple the measured values consistently overestimate the predictions by about 30 %. This is probably due partly to the rather unrepresentative nature of the measurements, and partly to the effects of wave reflection by the beach. In conclusion, despite the lack of representative sampling in some cases, the results are generally supportive of the two main theoretical predictions evident in figure 7, namely

(*a*) that the peak reflection coefficient increases linearly with the number of ripples; and

(*b*) that for a given number of ripples, and a given ripple steepness, the peak reflection coefficient increases both with increasing ripple amplitude and decreasing depth.

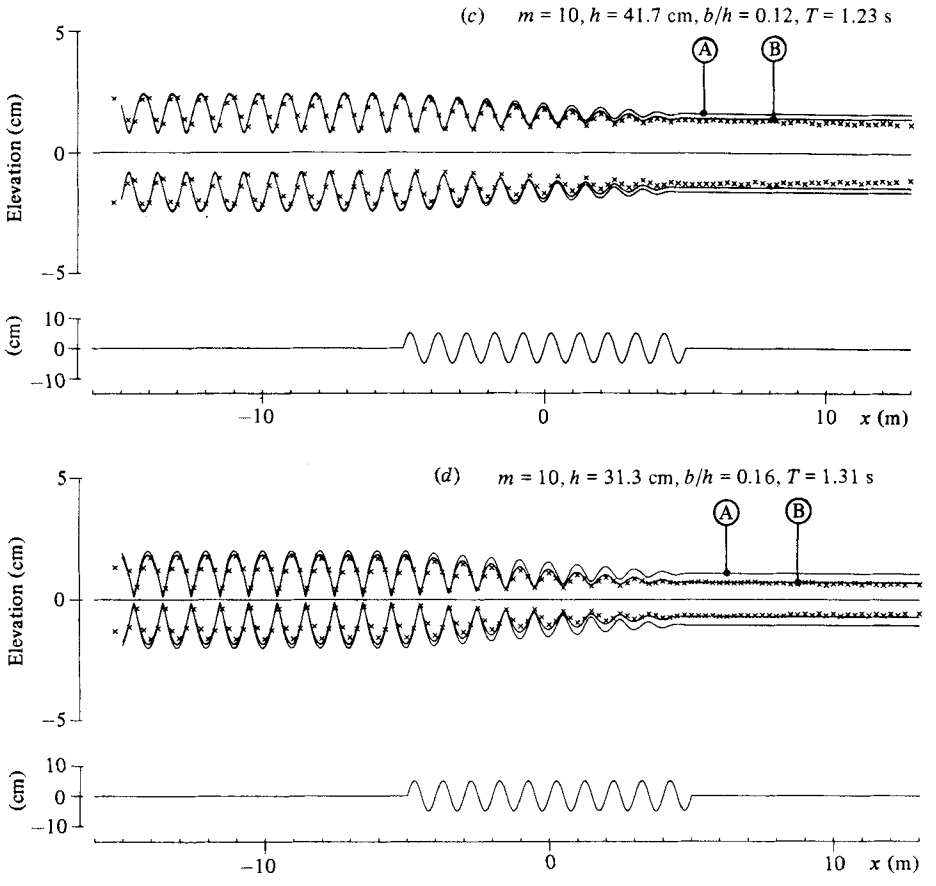

FIGURE 8. Variation of the amplitude of surface elevation throughout the wave tank at or near resonance ($2k/l \approx 1$), for different numbers m of ripples and different values of the quotient b/h of the ripple amplitude b and the water depth h. Curves A and B represent the wave envelopes given by the uncorrected and corrected theoretical results respectively (see §§2.2.2 and 4.2). T denotes the wave period.

4.2. *Measurements of surface elevation and reflection coefficient over, and on either side of, the ripple patch*

In order both to assess whether the measured values of $|K_R|$ discussed in §4.1 were truly representative of the reflection coefficient, and also to obtain a general understanding of the wave field, a series of measurements was made with the gauge configuration shown in figure 5(*b*), which was moved along the tank in steps of 1 m. Examples of the resulting measurements of the amplitude of surface elevation both above the ripple patch, and on either side of it, are shown in figure 8. The observations were made at or near the predicted resonant peak, and the measured surface elevations have been compared with predictions of elevation given by both the uncorrected and corrected theory. In each case, the incident-wave amplitude used in the comparisons has been obtained by averaging the first five values of $a_I (= a)$ determined from the measurements made on the upwave side of the ripple patch. The results for $m = 2$, 4 and 10 ripples show good agreement with the theory, and indicate clearly how the partially standing wave on the upwave side of the ripples gives way

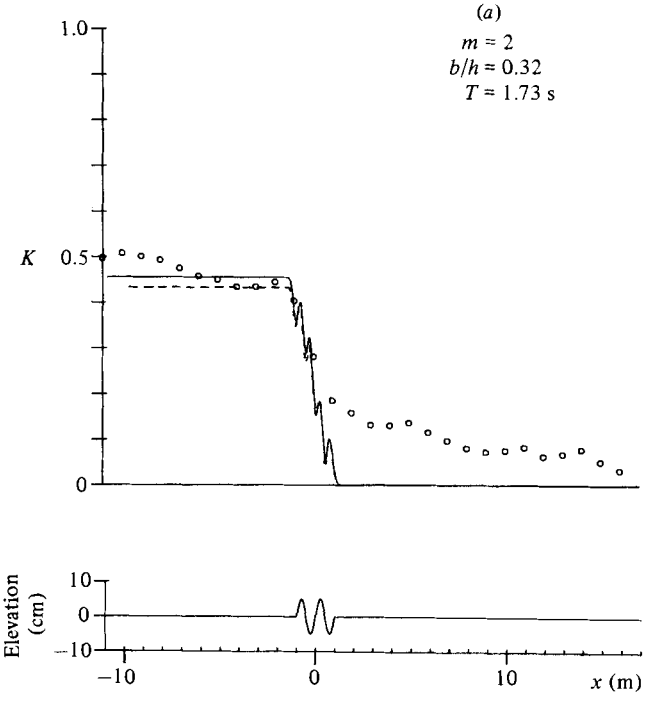

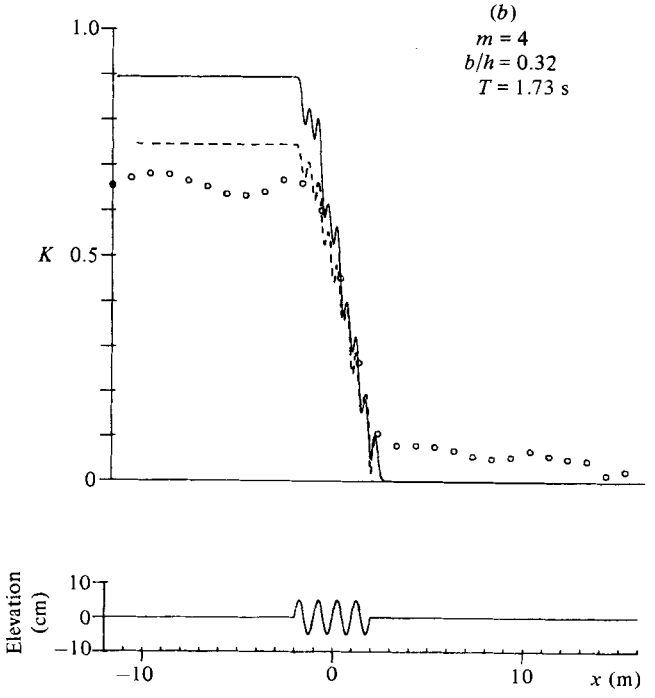

FIGURE 9(*a*,*b*). For caption see facing page.

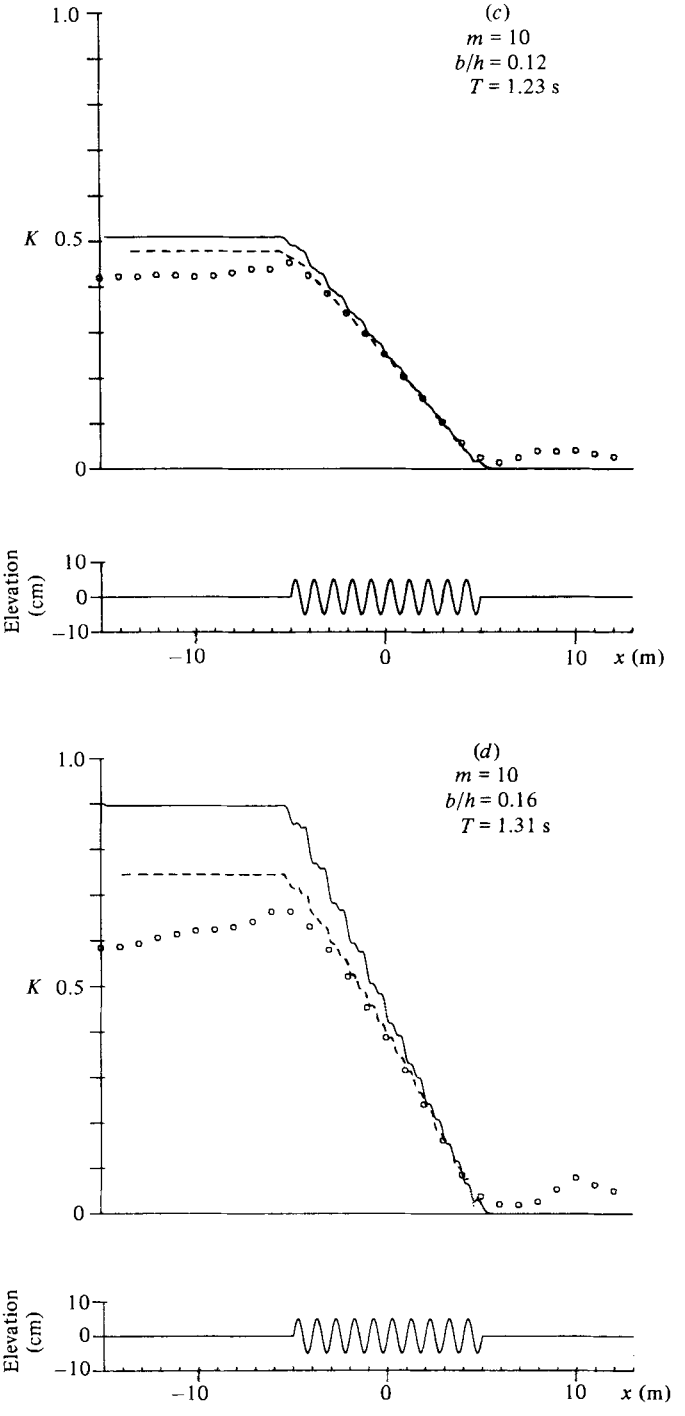

FIGURE 9. Variation of the wave-reflection coefficient K throughout the wave tank at or near resonance ($2k/l \approx 1$), for different numbers m of ripples and different values of the quotient b/h of the ripple amplitude b and the water depth h. Solid and broken curves represent the uncorrected and corrected theoretical results, respectively (see §§2.2.2 and 4.2). On the upwave side of the ripple patch, $K \to |K_R|$, the ripple reflection coefficient, while, on the downwave side, $K \to K_B$, the beach reflection coefficient. T denotes the wave period.

in a linear manner to a progressive wave on the downwave side (having an envelope comprising two parallel lines). On the downwave side, agreement is better between the measurements and the corrected, rather than the uncorrected, theory, as expected.

In general, good agreement has been found between the measured and predicted positions of the partially standing wave pattern (fixed in space) on the upwave side of the ripple patch. This may be seen in figure 8, where the phase angles of the measured and predicted envelopes of wave elevation are very similar. In most cases however, there is evidence of a small progressive phase shift of 1°–3° for each wavelength of the incident wave. For $m = 10$ ripples (figures 8*c*–*d*), this implies wavelengths in the experiments which were about 0.6–1.7 cm shorter than those predicted in the theoretical comparisons based on the nominal wave-period settings. Such discrepancies suggest true wave periods which were 0.002–0.006 s lower than the nominal values, for typical resonant waves with wavelength 200 cm in 50 cm depth of water. Since such differences are of the same order as those which were found in independent checks on the accuracy of the generated wave period (§3.2), the observed disagreements in phase may be accounted for by a small experimental error in the wave period setting. However, calculations for $m = 2$ and $m = 4$ ripples (figures 8*a*, *b*) suggest a greater mismatch, possibly of the order of 0.02–0.03 s in the wave-period setting. The reason for the poorer agreement in these cases is not clear.

Reflection coefficients calculated by the method of Goda & Suzuki (1977) are normally obtained from measurements made above flat beds, for which there is a fixed partitioning of the total wave energy into kinetic and potential energies. For waves of small amplitude, these two energies are equal, and results obtained for the reflection coefficient K, say, are independent of horizontal position x, at least if the wave measurements are made sufficiently far from the region of bed disturbance, or from the structure, being considered. If, however, measurements of elevation are made above an undulating bed, the partitioning of the total wave energy will depend upon horizontal position, and it follows that K will also depend upon position. Since this dependence may be rather complicated, a proper interpretation of K calls for a reliable theory for surface elevation as a function of position. Moreover, measured values of K will depend upon the gauge spacing. In the present context, what is obtained by the method of Goda & Suzuki is a modified reflection coefficient, which is such that $K \rightarrow |K_R|$ only on the upwave side of the ripple patch.

Figure 9 shows comparisons of measured and predicted reflection coefficients at resonance, both over the ripple patch and on either side of it, for $m = 2$, 4 and 10 ripples, and for different values of the ripple amplitude to water depth ratio. These typical examples are based on the measurements shown in figure 8. Agreement between observation and theory is generally good, the best agreement being achieved between the observations and the corrected, rather than the uncorrected theory. For $m = 10$ ripples (figures 9*c*, *d*), agreement is consistently good over the ripple patch. However, for large $|K_R|$ (figure 9*d*), the measured values of K underestimate the theoretical predictions on the upwave side, and overestimate them on the downwave side. It is possible that reflection of wave energy by the beach, which manifests itself in non-zero values of K on the downwave side, may have provided an unwanted contribution to the wave field on the upwave side. In particular, waves reflected by the beach may have interfered destructively with waves directly reflected by the ripples. By comparison, figure 9(*a*), for $m = 2$ ripples and $b/h = 0.32$, shows the measured reflection coefficients overestimating the theoretical values by significant amounts on the upwave side of the ripple patch, reasonable agreement being achieved

only over the ripple patch itself. This suggests that the wave reflected by the beach may lead to constructive, as well as destructive, interference effects. An alternative explanation for the more generally occurring underestimates in the measured values of $|K_R|$ on the upwave side (figures 9*c*, *d*) is that a non-negligible amount of available wave energy may have been dissipated in the tank. The general tendency for values of $|K_R|$ to decrease towards the wave generator is consistent with this explanation. This matter has been treated in detail by Davies & Heathershaw (1983) on the basis of estimates of the energy dissipated in the (laminar) boundary layers at the bed, and at the sidewalls, of the tank.

5. Discussion

5.1. *The validity of the comparisons*

Before the experiments described in §4 were carried out, it was necessary to establish that the waves generated in the tank complied with the limitations on the theory stated in §2.2.3 (equation (29)). Of these criteria, the one most easily violated was that involving the wave steepness ak. Typical wave steepnesses in the experimental runs were at the low end of the range $0 < ak \lesssim 0.16$, well within the limitation above. However, in order to establish whether variations occurred in the measured reflection coefficient on the upwave side of the ripple patch as the wave steepness increased, a series of tests was carried out with $m = 10$ ripples. For values of $|K_R|$ in the range 0–0.65, the amount of wave reflection remained relatively constant with increasing wave steepness, up to values of ak of about 0.16. The results of these tests have been presented by Davies & Heathershaw (1983).

As far as the two remaining criteria involving the wave amplitude a are concerned, the criterion involving a/h was well satisfied, since a/h was always less than 0.16 and was generally much smaller than this limiting value. The criterion involving the Ursell parameter a/k^2h^3 is actually less severe than indicated in (29), and may be expressed by $a/k^2h^3 \ll \frac{8}{3}$ (Davies 1982*b*). The largest value of the Ursell parameter in the present experiments was 0.44, for a limiting case in which the surface wavelength was very long ($\lambda_w \approx 400$ cm). More generally, for shorter surface wavelengths, its value was considerably less than this. Thus the three criteria involving the wave amplitude were well satisfied in the experiments. As a further check on this, the results of spectral analysis of the measured data were examined, in order to investigate the linearity of the measured wave field (see §5.2).

The remaining criteria in (29) involve the ripple amplitude b. Clearly, the ripple steepness bl was fixed by the chosen ripple geometry ($b = 5$ cm, $\lambda_R = 100$ cm), so that $bl = \frac{1}{10}\pi$. (This value was chosen because of its similarity to actual ripple and sandwave steepnesses.) The largest experimental value of the quotient b/h was 0.4, and the largest value of bk was about 0.39. While these values are perhaps larger than might have been desirable, the majority of the experiments were carried out with significantly smaller values. Moreover, as argued in §5.2, spectral analysis revealed that the wave field was almost always linear; this would not have been so if, for example, b/h had been too large.

A final limitation on the theory was that the flow above the rippled bed was always non-separating. This requirement was satisfied in all of the experimental runs described in §4. The criterion for non-separating oscillatory flow above a rippled bed is that the ripple wavelength λ_R is greater than the orbital excursion $2A_b$ of the water particles close to an equivalent flat bed ($A_b = U_b/\sigma$ and $U_b = gak/\sigma \cosh kh$) (Sleath 1975). In the present experiments, values of $2A_b/\lambda_R$ were generally $O(10^{-1})$, and

typically in the range 0.05–0.15. Although the dimensionless parameter $2A_b/\lambda_R$ takes no account of the presence of the evolving reflected wave over the ripple patch, it is clear that there was no possibility of separation in any of the experimental runs. This was confirmed by introducing dye into the flow in some selected cases.

5.2. *The linearity of the measured wave field*

Calculations of the reflection coefficient were generally made in such a way that the final results were relatively insensitive to any redistribution of wave energy from the fundamental frequency, into the first and higher harmonics (see Davies & Heathershaw, 1983). However, since the theory in §2 assumes a monochromatic wave field, the data was re-examined in a detailed way, in order to identify the presence of harmonics. This investigation revealed that, in the overwhelming majority of experimental runs, more than 95% of the total wave energy was at the fundamental frequency, most of the remainder being in the first harmonic. This provides a clear demonstration of the linearity of the wave field. However, in certain cases, rather less energy was found in the fundamental frequency; in particular, levels of 85–90% were measured in several runs. The reason for the presence of a significant first harmonic in these runs was examined in relation to various of the non-dimensional parameters in (29), namely ak, a/h, b/h and bk. However, detailed analysis of all the available data revealed no discernable reduction in the proportion of energy in the fundamental with increases in any of these parameters. Moreover, a similar investigation carried out in respect of the reflection coefficient of the beach also indicated no correlation of the kind sought. The only reasonably distinct correlation was between low proportions of energy in the fundamental and *low* values of the wave steepness ak. This rather unlikely result is probably explained by the inability of the wave gauges to resolve adequately very low waves. However, since there were many more runs at low wave steepness for which the wave field was essentially linear, this conclusion is, at best, tentative. The important point is that, for higher values of ak, a/h, b/h and bk, the wave field was linear, as required for meaningful comparisons with the theory.

5.3. *Implications of the results for sediment transport on an erodible bed*

The results described in §4 have significant implications for sediment transport on an erodible bed. For the simple case of a patch of sinusoidal ripples, it has been demonstrated that the reflection of incident waves at resonance ($k \approx \frac{1}{2}l$) gives rise to a partially standing wave pattern on the upwave side of the ripple patch (see figures 4 and 8). If the bed is erodible, this suggests the possible development of new ripples on the upwave side of the patch, having the same wavelength as the existing ripples. Intuition suggests that accumulation of material will occur beneath antinodes of elevation, and that erosion will occur beneath nodes, though the situation may be complicated by the residual circulation cells which result from bottom friction under a partially standing wave structure (see Davies & Heathershaw 1983, §4.4). Previous observations of sand movement on a flat erodible bed beneath a partially standing wave structure have been made in the laboratory by Kennedy & Falcón (1965). However, the situation described by these workers was rather different from that in the present experiments, largely on account of the fact that their observations were made in far more active flow conditions. More recently, Nielsen (1979) has demonstrated ripple growth beneath standing waves, with sediment accumulation occurring at the antinodes of surface elevation.

In order to examine the possible development of new ripples upwave of the existing

ripple patch, a single trial was carried out for a near-resonant case, in which a thin veneer of sand (mean diameter 235 μm) was distributed throughout the fixed ripple patch and on either side of it. The details of this exercise have been discussed fully by Davies & Heathershaw (1983). It was observed that there was a tendency for new ripples to grow in those regions of the bed in $x < -L$ with relatively small bottom velocity amplitudes, that is in regions of the bed beneath the antinodes of elevation. In particular, on the basis of a comparison between the predicted distribution of bottom velocity amplitudes and the known sediment threshold velocity amplitude, the observed regions of incipient ripple growth coincided quite closely with predicted regions of relatively small bottom velocity amplitude. A clear implication of this is that, in general, there may be a coupling between wave reflection and ripple growth on an erodible bed. However, for there to be such a coupling, accumulation and erosion must occur on the *existing* ripple patch in a manner which suggests ripple growth, rather than erosion, by the wave action. Unfortunately, it was unclear from the present single trial whether, in general, an existing ripple patch is likely to be a stable, or an unstable, feature on the bed, particularly in resonant cases in which there is a significant amount of wave reflection. One complicating factor is the effect of variable grain size. In a related study involving a partially standing wave pattern above a rippled bed, Scott (1954) observed a tendency for coarser grains to be found in the region of the ripple crests, and for finer grains to be found in the region of the troughs. Such a grain-size distribution clearly affects the stability of the bed. This matter calls for further theoretical and experimental investigation.

6. Conclusions

Measurements in a wave tank have confirmed the principal conclusions of the studies of Davies (1980, 1982*a*) concerning the reflection of wave energy by a patch of sinusoidal ripples on an otherwise flat bed. Firstly, it has been demonstrated that, for a given number of ripples in the patch, the reflection coefficient is oscillatory in the quotient of the surface (k) and ripple (l) wavenumbers, as expected from (25). Secondly, it has been demonstrated that a resonant interaction occurs when $2k/l \approx 1$, associated with which there may be a significant amount of wave reflection. At resonance, the reflected wave amplitude increases linearly with the number of ripples in the patch (equation (26)). Moreover, for a given number of ripples, and a given ripple steepness, the reflection coefficient increases both with increasing ripple amplitude and decreasing depth.

Agreement between theoretical predictions and experimental results has been found to be generally good also in comparisons made in resonant cases between the predicted and measured wave fields over the ripple patch itself. It has been demonstrated that the transition from a partially standing-wave pattern upwave of the ripple patch, to a purely progressive (outgoing) wave on its downwave side, is accomplished in an almost linear manner over the full extent of the ripple patch. This fact has been exploited in the procedure adopted in §2 to ensure a balance between the energy fluxes associated with the incident, reflected and transmitted waves.

It was suggested by Davies (1980, 1982*a*) that the partially standing wave formed in resonant cases on the upwave side of the ripple patch might lead, on an erodible bed, to the growth of the ripple patch in the upwave direction. An experiment carried out with sand in the wave tank has shown that areas of preferential erosion and deposition do indeed occur on the upwave side of the ripple patch, and that the distance between areas of deposition is equal to the original ripple spacing. Potentially,

at least, resonant interaction between surface waves and bottom undulations provides a mechanism for the growth of a ripple patch in the upwave direction, though further studies of the stability of the bedforms are required. The possibility of a coupling between wave reflection and ripple growth has significant implications for aspects of coastal protection.

We are grateful to the Commander and Director of the US Army Corps of Engineers, Coastal Engineering Research Center, Fort Belvoir, Virginia, USA, for providing experimental facilities. We are grateful also to Professor T. V. Davies for his valuable comments on aspects of the theory in §2.

Computer programming and analyses were carried out by Mrs D. J. Corns, illustrations were prepared by Mrs C. D. Kemp and the paper was typed by Mrs J. Reeves and Mrs M. Ridge.

REFERENCES

Beckmann, P. & Spizzichino, A. 1963 *The Scattering of Electromagnetic Waves from Rough Surfaces*. Pergamon.

Dalrymple, R. A. & Fowler, J. F. 1982 Bragg scattering by pile-supported structures. *J. Waterway, Port, Coastal and Ocean Div. ASCE* **108** (WW3), 426–429.

Davies, A. G. 1980 Some interactions between surface water waves and ripples and dunes on the seabed. *Inst. Oceanogr. Sci. Rep.* 108.

Davies, A. G. 1982*a* The reflection of wave energy by undulations on the seabed. *Dyn. Atmos. Oceans* **6**, 207–232.

Davies, A. G. 1982*b* On the interaction between surface waves and undulations on the seabed. *J. Mar. Res.* **40**, 331–368.

Davies, A. G. & Heathershaw, A. D. 1983 Surface wave propagation over sinusoidally varying topography: theory and observation. *Inst. Oceanogr. Sci. Rep.* 159.

Fitz-Gerald, G. F. 1976 The reflexion of plane gravity waves travelling in water of variable depth. *Phil. Trans. R. Soc. Lond.* A **284**, 49–89.

Fortuin, L. 1970 Survey of literature on reflection and scattering of sound waves at the sea surface. *J. Acoust. Soc. Am.* **47**, 1209–1228.

Goda, Y. & Suzuki, Y. 1977 Estimation of incident and reflected waves in random wave experiments. In *Proc. 15th Intl Conf. on Coastal Engng, 1976*, pp. 828–845. ASCE.

Heathershaw, A. D. 1982 Seabed-wave resonance and sand bar growth. *Nature* **296**, 343–345.

Jeffreys, H. 1944 Motion of waves in shallow water. Note on the offshore bar problem and reflexion from a bar. *Ministry of Supply Wave Rep.* 3 (London).

Kellum, F. W. 1956 An electronic gage for measurement of small waves and ripples. *Bull. Beach Erosion Board, US Army Corps of Engrs* **10**, 32–40.

Kennedy, J. F. & Falcón, M. 1965 Wave-generated sediment ripples. *MIT Dept Civ. Engng, Hydrodyn. Lab. Rep.* 86.

Kreisel, G. 1949 Surface waves. *Q. Appl. Maths* **7**, 21–44.

Lamb, H. 1932 *Hydrodynamics*, 6th edn. Cambridge University Press.

Langhorne, D. N. 1982 A study of the dynamics of a marine sandwave. *Sedimentology* **29**, 571–594.

Long, R. B. 1973 Scattering of surface waves by an irregular bottom. *J. Geophys. Res.* **78**, 7861–7870.

Mei, C. C. & Black, J. L. 1969 Scattering of surface waves by rectangular obstacles in waters of finite depth. *J. Fluid Mech.* **38**, 499–511.

Mitra, A. & Greenberg, M. D. 1984 Slow interactions of gravity waves and a corrugated seabed. *Trans. ASME* E: *J. Appl. Mech.* (in press).

Newman, J. N. 1965 Propagation of water waves past long two-dimensional obstacles. *J. Fluid Mech.* **23**, 23–29.

NIELSEN, P. 1979 Some basic concepts of wave sediment transport. *Tech. Univ. Denmark, Inst. of Hydrodyn. and Hydraul. Engng. Series Paper* 20.

PEREGRINE, D. H. 1972 Equations for water waves and the approximations behind them. In *Waves on Beaches* (ed. R. E. Meyer), pp. 95–121. Academic.

SCOTT, T. 1954 Sand movement by waves. *US Army Corps of Engrs, Beach Erosion Board, Tech. Memo.* 48.

SHORT, A. D. 1975 Multiple offshore bars and standing waves. *J. Geophys. Res.* **80**, 3838–3840.

SLEATH, J. F. A. 1975 Transition in oscillatory flow over rippled beds. *Proc. Inst. Civ. Engrs* **59**, 309–322.

STAFFORD, R. B. 1972 Investigation and procedure for calibration of CERC laboratory wave gage FWK Model-1. Washington, DC, Coastal Engng Res. Center (unpublished document).

URSELL, F. 1947 The reflection of waves from a submerged low reef. *Admiralty Res. Lab., Teddington, Middx, Rep.* ARL/R5/103.41/W.